Rev.Adv.Mater.Sci. 21(2009) 57-74

CHARACTERISATION AND MODELLING OF METAL DEPOSITION IN CATALYTIC COMPOSITE MEMBRANES

N. Wehbe[1], A. Bonilla Sanchez[2], J.-A. Dalmon[1], N. Guilhaume[1], N. Homs[2], Y. Li[3], S. Miachon[1] and P. Ramirez de la Piscina[2]

[1]Institut de Recherches sur la Catalyse et l'Environnement de Lyon (IRCELYON), UMR 5256 CNRS-Université Claude Bernard Lyon 1, 2 Avenue Albert Einstein, F-69626 Villeurbanne Cédex, France
[2]Departament de Qui´mica Inorganica, Universitat de Barcelona, Marti i Franques 1-11, 08028 Barcelona, Spain
[3]Present address: School of Materials Science and Engineering, East China University of Science and Technology, 130 Meilong Road, Shanghai 200237, China

Received: July 12, 2008

Abstract. A wet impregnation technique based on the evaporation-crystallisation method was used to prepare mono- and bi-metallic catalytic membranes, using Al_2O_3 or TiO_2 multilayer porous tubes with a top-layer pore size of 5, 10, 25, 30 or 100 nm. The metal deposition was characterized by weight uptakes, chemical analyses, SEM-EDS and XPS analyses. In all tubes with a mesoporous top-layer bearing pores of 5, 10 or 25 nm, whatever the nature of the tube and the impregnation solvent (water or acetone), a strong metal enrichment was evidenced in the top-layer. This enrichment was less noticeable in tubes with a 30 or 100 nm top-layer pore size. A mathematical model describing the metal salts deposition during the drying step is proposed. This model is discussed in relation with the physical parameters involved in the drying of complex porous systems.

1. INTRODUCTION

Bimetallic catalysts are widely used in the fields of hydrogenation, fine chemistry, selective oxidation and many others. The beneficial presence of a co-metal can be interpreted in terms of geometric (dilution), electronic, and/or mixed sites effects.

Pd-Cu bimetallic catalysts are very active in the catalytic hydrogenation of nitrates in aqueous solution. Copper has been identified as the active element for primary nitrates (NO_3^-) reduction into nitrites (NO_2^-) by a redox mechanism, whereas Pd achieves the final reduction of nitrites into N_2 [1]. The Pd/Cu ratio has a decisive effect on activity and selectivity, the optimum atomic ratio being close to 2 [2]. However, the catalytic activity is often limited by diffusion, whereas undesirable NH_4^+ can be formed as by-product. In order to improve the activity and to control the reaction selectivity towards N_2, catalytic membrane contactors represent a promising alternative to conventional reactors [3].

Similarly, Pd-Zn catalysts have been identified as efficient catalysts for the direct dehydrogenative dimerization of ethanol to produce ethyl acetate in a single step [4], avoiding handling corrosive or toxic reactants. The high activity of the Pd-Zn bimetallic catalyst was related to the formation of an alloyed Pd-Zn phase.

Catalytic membrane reactors (CMRs) combine, in the same unit, a conversion effect (catalyst) and a separation effect (membrane). These reactors, beside the obvious interest of coupling two classi-

Corresponding author: N. Guilhaume, e-mail: Nolven.Guilhaume@ircelyon.univ-lyon1.fr

Table 1. Main characteristics of the Pall-Exekia multilayered alumina supports.

Membrane	**Layer number** (material) Thickness (μm) / Mean pore size (nm)			
	1 (α-Al_2O_3)	**2** (α-Al_2O_3)	**3** (α-Al_2O_3)	**4** (γ-Al_2O_3)
Al_2O_3 - 25 nm	1500 / 12000	30 / 800	15 / 200	2 / 25
Al_2O_3 - 10 nm	1500 / 12000	30 / 800	15 / 200	2 / 10
Al_2O_3 - 5 nm	1500 / 12000	30 / 800	15 / 200	2 / 5

cal steps of chemical processes in the same unit, have already shown various potential benefits for a range of catalytic reactions [5].

If the deposition of a single metal in ceramic membranes by standard methods like impregnation is well described, the deposition of two metals in a controlled ratio is less trivial: differences in precursors solubility, and liquid transfer within the pores due the capillary pressure, can contribute to an uneven metal distribution [6]. In the case of strongly anisotropic supports like the multilayered ceramic tubes used in the present study, liquid transport will take place from the large to the small pores during drying, leading to metal concentration in the porous layer with the smallest pore size [7]. Controlling the deposition of two metals for a close contact between the metals or in a specific ratio is difficult, since the precipitation zone will depend on the precursor solubility.

To overcome these issues, Pd-Cu bimetallic catalysts on ceramic membranes were prepared by MOCVD methods by Daub *et al.*, starting from volatile organometallic Pd and Cu precursors [8]. The technique, however, is costly and time consuming. Several preparation techniques were used to prepare catalytic membranes. The characterisation of metal deposits, however, is often performed on a global scale. Ilinitch *et al*. [9] prepared bimetallic Pd-Cu disk-shaped membranes by *in-situ* reduction of palladium chloride and copper nitrate with sodium borohydride. Only the global composition of the membrane was characterised. In-situ chemical reduction of Pd salts was also used to deposit Pd in polypropylene hollow fibre membranes [10]. The choice of an alcohol as the reducing agent allowed the deposition of well-distributed Pd particles over the entire polymer surface area. More complex methods like layer-by-layer adsorption of polyelectrolyte/metal colloids were investigated [11]. This method allowed controlled deposition of polymer-stabilised gold nanoparticles on porous alumina membranes. The evaporation-crystallisation technique was also applied to the deposition of hexachloroplatinic acid in commercial ceramic tubes [12]. This simple method is directly related to the classical wet or incipient wetness impregnation techniques, often used to prepare supported metal catalysts. SEM/EDX line-scan analyses showed that Pt was mainly concentrated in the mesoporous zirconia top-layer of the tube, although some large Pt particles were also observed in the TiO_2-modified Al_2O_3 macroporous layers.

In the present work, the preparation of bimetallic catalysts deposited on porous ceramic membranes by the evaporation - crystallization method has been investigated. The membranes have been characterised by different techniques, and a model describing the metals deposition is proposed.

2. EXPERIMENTAL

2.1. Materials

Commercial tubular alumina porous supports (T1-70, Pall-Exekia) were used in this study (outer diameter 10 mm; inner diameter 7 mm, length 250 mm, with 10 mm enamelled endings). The tubes are made of 4 concentric alumina layers with decreasing pore size from external to internal sides (Table 1). The γ-Al2O3 top layer is mesoporous, with an average pore size of 5, 10 or 25 nm.

The porous TiO_2 supports were supplied by Inocermic. They display the same dimensions as the alumina supports, and also consist in several concentric TiO_2 layers whose pore size decreases from the outside to the inside part, the number of layers depending of the smallest pore size (Table 2). TiO_2 membranes with a pore size of the top layer of 100, 30, and 5 nm were used.

Table 2. Characteristics of the Inocermic multilayered supports TiO_2-5 nm, TiO_2-30 nm and TiO_2-100 nm.

Membrane	Layer Thickness (mm) / Mean pore size (nm)				
	1	**2**	**3**	**4**	**5**
TiO_2-100 nm	1500 / 5000	46 / 800	27 / 250	10 / **100**	-
TiO_2-30 nm	1500 / 5000	46 / 800	27 / 250	8 / **30**	-
TiO_2-5 nm	1500 / 5000	46 / 800	27 / 250	8 / 100	0.5 / **5**

2.2. Membranes preparation

Monometallic and bimetallic membranes were prepared by the evaporation-crystallization method, by single step or successive impregnation.

Pd-Cu/Al_2O_3 membranes

$Pd(NO_3)_2$ (10 wt.% in aqueous 10 wt.% HNO_3, Aldrich) and $Cu(NO_3)_2 3H_2O$ (Aldrich) were used as precursors and dissolved in water. Several solutions with different Pd/Cu ratios were used for impregnation of alumina tubes. The tube was rotated vertically in this solution for 15 h, then removed and dried at room temperature in horizontal position under rotation (60 rpm) for 24 h. The metals were directly reduced under hydrogen at 250 °C for 15 h (heating rate 1 °C/min).

Pd and Pd-Zn/TiO_2 membranes

An acetone solution (0.75 g of Pd/L) of $Pd(CH_3COO)_2$ (Acros 47.5% Pd) was used for the impregnation (the solubility in acetone is 0.22 M at 25 °C [13]). The membrane was sunk at room temperature in the precursor solution and stirred vertically for 24 h. The tube was removed from the solution and two stoppers were inserted in each side of membrane. Then, it was placed in a large bottle containing acetone vapour (to favour the slow evaporation of the solvent, since acetone evaporates rapidly) and was horizontally spun (60 rpm) for 24 h at room temperature for drying. Then, the membrane was additionally dried at 100 °C for 12 h and weighed. Calcination was carried out in an oven at 300 ºC for 2 h with 60 ml/min of flowing air. Afterwards, the membranes were reduced in 60 ml/min of flowing H_2 at 250 °C for 2 h.

The membranes containing palladium and zinc were first impregnated by Zn, then by Pd. A zinc acetate aqueous solution was used for Zn impregnation. The tube was stirred in the precursor solution for 24 h at room temperature, then dried horizontally at room temperature with stirring for 24h, followed by calcination in air at 300 °C to decompose zinc acetate. Pd acetate was deposited consecutively as described previously.

2.3. Characterisations

Nitrogen permeation measurements were performed before and after metals deposition using a conventional setup [7]. For chemical analysis, the tubes were broken and selected pieces were crushed into a powder. Chemical analyses were performed by Inductively Coupled Plasma (ICP) after dissolution of the crushed membrane pieces in a mixture of strong acids (H_2SO_4 + HNO_3 + HF, followed by HCl + HNO_3). This treatment left a very small amount of white insoluble powder, which probably consists in α-Al_2O_3. The analyses were obtained on the soluble part.

For scanning electron microscopy (SEM) examination and analysis, the membrane was broken, and small parts of tube were used stuck on the sample holder. The characterisation of titaniabased membranes by electron probe microanalysis (EPMA-EDX) was performed with an EPMA-WDX CAMECA SX-50 microscope equipped with Wavelength Energy Dispersive X-ray (WDX) and Energy Dispersive X-ray (EDX) spectrometers with 1 to 2 μm resolution, accelerating voltage of 20 kV and current of 20 nA. The microanalysis study was carried out on small membrane pieces, which were polished and covered with a polymer. The probe was displaced by steps of 1 μm along the membrane cross-section.

A FEI XL30 ESEM-FEG microscope coupled to an energy dispersive X-ray spectroscopy system was used to investigate the metals distribution on the surface and in cross-sections of alumina-

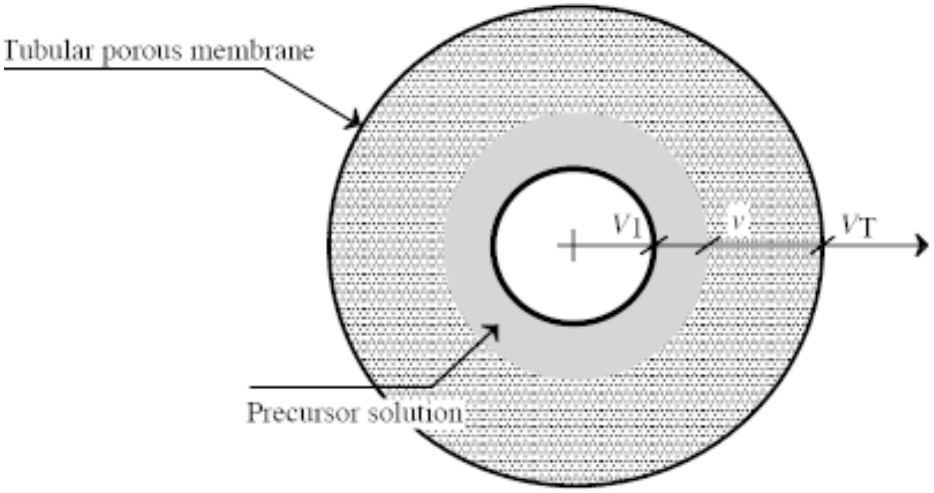

Fig. 1. Cross section of the tube at a given time of the evaporation process, before saturation.

based membranes. Since there is no charging on non-conductive samples in an ESEM microscope, the samples did not require polishing and covering by a conductive film, and were directly examined. The EDS probe size was about 2x2 μm, and the depth analysed about 1 μm. However, this size is in the same order of magnitude as the pore size of the macroporous layers of the tubes, which leads to uncertainty in the measurements in these zones. Therefore, EDS analyses were considered as only semi-quantitative on alumina-based membranes.

X-ray photoelectron spectra were recorded on membrane pieces placed in the sample holder of a VG Scientific ESCALAB 200R spectrophotometer. The thickness of the analyzed area was ≈ 5 nm.

3. MODEL FOR METALS DEPOSITION BY EVAPORATION-CRYSTALLISATION

A model describing a single metal deposition in a similar membrane has been proposed earlier [7]. Basically, it is assumed that the solvent will evaporate first in the larger pores of the tube, leading to a migration of the solution towards the smaller pores. Accordingly, the model calculates a distribution function C_e of solid particles as a function of the variable volume *v*, which represents the volume concentration of metal deposited in the membrane thickness by evaporation of a soluble precursor solution (Eq. (1).

$$C(v) = \rho . C_s^* . \ln \frac{V_s - V_1}{v - V_1} \quad (1)$$

with:
v: volume variable,
C(v): metal particle concentration in the membrane after deposition,
ρ: membrane porosity,
C_s*: saturation concentration in the liquid (concentrations in liquids are indicated by *),
V_s: value of *v* corresponding to the saturation volume,
V_1: value of *v* corresponding to lumen volume of the membrane tube.
The different parameters are represented on Fig. 1.

In the present work, this approach was applied to two metals deposited simultaneously but independently from each other. This model was also developed in order to take into account the possible loss of metal precursor before the evaporation reaches V_s (for example deposited in small non-connected dead-end pores, or on the external surface of the support due to very fast evaporation). A parameter, *l,* was added in Eq. (1) to take this loss into account, leading to Eq. (2):

$$C(r) = l\rho C_S^* \ln \frac{R_S^2 - R_1^2}{r^2 - R_1^2} \quad (2)$$

with:
l: metal precursor loss coefficient,
r: radius variable,

Table 3. Catalytic membranes prepared.

Sample reference	Support type	Metals deposited	Deposition method	Metal precursors
1-Al-5nm	Al_2O_3 – 5 nm	Pd + Cu	Single step	Pd and Cu nitrates
2-Al-10 nm	Al_2O_3 – 10 nm*	Pd + Cu	Single step	Pd and Cu nitrates
3-Al-10 nm	Al_2O_3 – 10 nm*	Pd + Cu	Single step	Pd and Cu nitrates
4-Al-25 nm	Al_2O_3 – 25 nm	Pd + Cu	Single step	Pd and Cu nitrates
5-Ti-5 nm	TiO_2 – 5 nm	Pd	Single step	Pd acetate
6-Ti-5 nm	TiO_2 – 5 nm	Pd	Single step	Pd acetate
7-Ti-30 nm	TiO_2 – 30 nm	Pd	Single step	Pd acetate
8-Ti-100 nm	TiO_2 – 100 nm	Pd	Single step	Pd acetate
9-Ti-5 nm	TiO_2 – 5 nm	Zn + Pd	Successive deposition	Pd and Zn acetates

* The samples prepared on alumina supports with 10 nm pores were prepared on sections of tube of ≈ 6 cm length, with different Pd/Cu ratios in the impregnation solution.

Table 4. Nitrogen permeance of the bare and impregnated tubes.

Sample	Permeance to nitrogen ($mmol \cdot m^{-2} \cdot s^{-1} \cdot Pa^{-1}$)	
	Bare support	Support after metal deposition
1-Al-5 nm	8.3	7.6
4-Al-25 nm	28	29
5-Ti-5 nm	32	30
6-Ti-5 nm	33	30
7-Ti-30 nm	21	20
8-Ti-100 nm	32	30

C(r): metal particle concentration in the membrane after deposition,
R_s: value of *r* corresponding to the saturation volume,
R_1: value of *r* corresponding to lumen volume of the membrane tube (internal tube radius).

In Eq. (2), the variables were translated into radius rather than volume for practical reasons. As a matter of fact, this equation was compared to the data obtained from EDX spatial analysis of metals along the membrane thickness.

4. RESULTS

4.1. Samples prepared

Several membranes were prepared, varying the nature of the tube (Al_2O_3 or TiO_2) and the pore size, the metals concentration and ratios in the precursor solutions, and the deposition in one or two steps. Most samples were prepared on full-length tubes, except for samples 2-Al-10 nm and 3-Al-10 nm, which were prepared on short sections of tube using the same procedure. The metals were deposited by single-step impregnation for most samples except the bimetallic Pd-Zn membrane (Table 3). Alumina-based membranes were prepared using metal nitrates precursors, whereas metal acetates were used in the case of titania-based tubes.

4.2. Nitrogen permeance.

The nitrogen permeance was measured on the tubes before and after metals deposition, in order to check any plugging of the porosity. As can be seen in Table 4, the permeance does not change significantly after metals deposition.

4.3. Quantification of metal loading by deposition-precipitation

This part presents weight uptake measurements and chemical analyses of precursor solutions and

Table 5. Amounts of metal deposited in the membranes (in mg metals in a 25-cm long tube) determined by chemical analyses on crushed pieces of tube, and by measured and calculated weight uptakes.

Sample	Metal concentrations in precursor solution (g/L)	Pd (mg) chemical analysis	Cu (mg) chemical analysis	Pd + Cu (mg) chemical analysis	Pd + Me (Cu or Zn) (mg) weight uptake	Pd + Me (Cu or Zn) (mg) calculated weight uptake[b]
1-Al-5 nm middle	8.7 (Pd)	16.3	8.6	24.9	35	40.8
1-Al-5 nm end	4.5 (Cu)	19.5	9.9	29.4		
2-Al-10 nm[a]	9.3 (Pd) 2.14 (Cu)	35.8	11.9	47.7	33.2	38.4
3-Al-10 nm[a]	9.9 (Pd) 1.57 (Cu)	45.1	10.9	56	38.7	44.0
4-Al-25 nm	9.2 (Pd) 2.15 (Cu)	32.8	6.6	39.4	48.6	39.8
5-Ti-5 nm	0.86 (Pd)	n. a.	-	-	3.7	2.5
6-Ti-5 nm	2.17 (Pd)	n. a.	-	-	7.3	6.2
7-Ti-30 nm	1.11 (Pd)	n. a.	-	-	3.6	3.0
8-Ti-100 nm	1.18 (Pd)	n. a.	-	-	3.9	3.0
9-Ti-5 nm	1.28 (Pd) 5.65 (Zn)	n. a.	n. a.	-	5.7 (Pd) 30.6 (Zn[c])	3.6 (Pd) 18.1 (Zn)

[a]for these samples prepared on sections of tube, the values in the table are normalised to a total length of 23 cm (corresponding to a 25-cm tube minus enamel endings).
[b]calculated from the concentration of metal precursors in the solution and the porous volume of the tube.
[c]calculated from Δm supposing the formation of ZnO after calcination of zinc acetate.
n. a.: not analysed.

material. Since chemical analysis of material requires breaking the tube, only a limited number of samples were analyzed by this method. Analyses of the Pd and Cu contents in the membrane were performed on crushed pieces of tube. The expected mass of metals in the tubes was also calculated from the porous volume of each tube and the concentration of metal salts in the precursors solution (Table 5).

For the Al_2O_3–5 nm membrane, chemical analyses of metals were performed on pieces originating from two different positions of the tube (middle and end). Similar Pd and Cu amounts were found in both parts of the tube, which suggests that the metals deposition is homogeneous in the axial direction of the tube. Therefore, the chemical analyses performed on pieces of tube crushed into a powder were considered representative of the Pd and Cu compositions in the whole tube. The amounts of Pd and Cu deposited in a tube calculated from chemical analyses can be considered to agree fairly well with those determined by weight uptake, within the uncertainties related to their representation of the whole tube composition and to the accuracy of both measurements.

As far as alumina supports are concerned, the weight uptake measured also agrees relatively well with the calculated weight uptake. With the titania tubes, however, the measured weight uptake is always higher than that expected from calculation. This difference may arise from residual carbon originating from the metal acetate precursors: although zinc acetate decomposes at 237 °C [14] and palladium acetate between 195 and 240 °C [15], calcining the tube at 300 °C in air may be too low temperature to fully burn the carbonaceous residues trapped in the membrane pores.

During the drying of impregnated membranes, capillary forces will redistribute the solution of metal precursors from large to small pores (i.e. in the radial direction of the tube). This should lead to a concentration of the metal precursors in the mesoporous layer of the membrane, which in the present case is the inner side of the tubes [6,7]. In

Table 6. Chemical analyses (global and scraped zones, shown in grey) of membrane 1-Al-5 nm (in mg metals in a 25-cm long tube). The last line describes the amount of metals deposited per μm of membrane thickness.

Scraped zone	Inside	Intermediate 1	Intermediate 2	Outside	Global
Equivalent thickness (μm)	20	80	1100	300	1500
Pd mass (mg)	8	1.2	4.6	4.4	17.9
Cu mass (mg)	6	4.5	1.5	5	9.2
Distribution (mgPd+ Cu/μm)	0.7	0.07	0.005	0.03	0.02

Table 7. Chemical analyses (global and scraped zones) of membrane 4-Al-25 nm (in mg metals in a 25-cm long tube).

Scraped zone	Inside	Intermediate	Outside	Global
Equivalent thickness (μm)	40	1380	80	1500
Pd mass (mg)	3	19	3.7	32.8
Cu mass (mg)	0.6	3.8	0.8	6.6
Distribution (mg Pd+ Cu/μm)	0.09	0.016	0.056	0.026

order to check the distribution of metals in the thickness of the tubes, thin zones of material were scraped off the inner and outside sides of the tubes as powders, and the Pd and Cu contents were analyzed by ICP. The remaining part was crushed into a powder and also analyzed. Knowing the density of porous alumina, the mass of each scraped sample was used to calculate an equivalent thickness. For comparison, global analyses of Pd and Cu contents were also performed on pieces cut in the tubes in the radial direction and crushed. The results are shown in Table 6 and Table 7. Since some of the scraped samples correspond to very small amounts, the metals mass balance between the scraped samples and the global analyses is only approximate. Nevertheless, these analyses evidence strong variations of metals distribution in the membrane thickness (last lines of Tables 6 and 7), since the values display large differences.

The zones scraped on the inner side of the tubes (which removed the mesoporous γ-Al_2O_3 layer of ≈2 μm thickness) are clearly more loaded in metals than the other layers, on a thickness basis, which confirms the concentration of metal precursors during the drying process. The outside layer is also enriched in metals, although to a lesser extent, because some evaporation of the precursors solution also takes place directly from the outside of the tubes.

Fig. 2 compares the Pd/Cu ratios obtained from chemical analyses of the tube (global and scraped zones) with the Pd/Cu ratio in impregnation solutions. Although some analyses of scraped zones should only be considered as indicative, because of large experimental errors (low metal amounts, few samples collected for analyses…), they suggest that the Pd/Cu ratios vary significantly in the membrane thickness (radial direction). They also

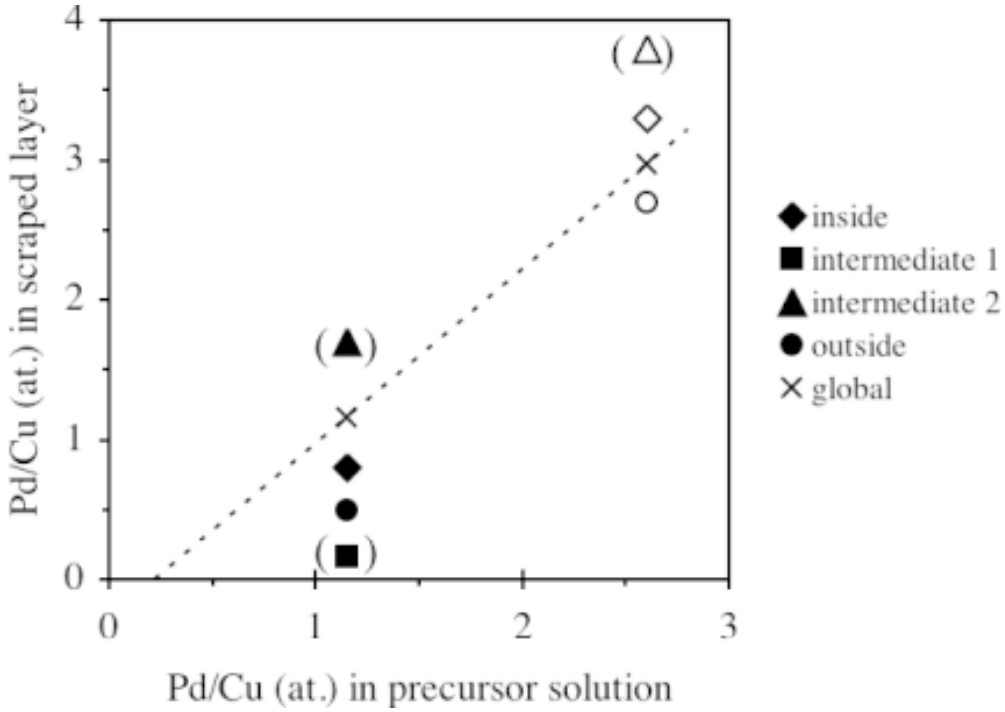

Fig. 2. Comparison of Pd/Cu atomic ratios in impregnation solution with Pd/Cu ratios analyzed in the tubes (global and scraped zones). Full symbols: 1-Al-5 nm sample, open symbols: 4-Al-25 nm sample. Symbols in brackets refer to samples in which one of the metals was analyzed in very low amounts (<0.02 wt.%).

differ from the Pd/Cu ratio in the precursors solution. Nevertheless, the Pd/Cu ratios calculated from global analyses of the tubes are consistent with those in the precursor solution.

4.3.1. Analysis of metals deposition by SEM-EDS

4.3.1.1. Single metal (Pd) membranes

This section presents the distribution of metals in the membranes cross-section analysed by EDS. The model presented in section 3 was used to draw the theoretical curves of metal deposition and estimate the values of parameter *a*.

Pd/TiO_2-5 nm membranes

The Pd deposition profile analysed in the cross-section of the 5-Ti-5nm membrane (prepared with a Pd concentration in the impregnation solution of 0.86 g/L) is shown in Fig. 3.

Most of palladium was deposited in 15-20 μm depth. The mean integral of the experimental curve (microanalysis) was determined. Up to 27 μm depth, a palladium content of 0.26 wt.% was found. The palladium content when the whole membrane (1600 μm) was considered was 0.005 wt.%. Comparison with the model curve integral (Fig. 3) indicated a palladium deficiency of 40 wt.%.

The Pd deposition profile in the cross-section of the 6-Ti-5nm membrane (prepared with a Pd concentration in the impregnation solution of 2.17 g/L) is shown in Fig. 4.

Similarly, most of the Pd is deposited in the first 10 μm from the mesoporous top-layer. In this zone, the Pd concentration is roughly double from that in sample 5-Ti-5nm.

Pd/TiO_2-30 nm and Pd/TiO_2-100 nm membranes

In Figs. 5 and 6, the palladium deposition profiles obtained by microanalysis and the adjusted mathematical model are shown.

In both cases, an almost homogeneous deposition was analyzed within the whole membrane thickness. Only a very moderate Pd concentration was observed within the first 40 μm depth. The palladium determined over the whole membranes was 0.002 and 0.003 wt.% in Pd-TiO_2-30 nm and

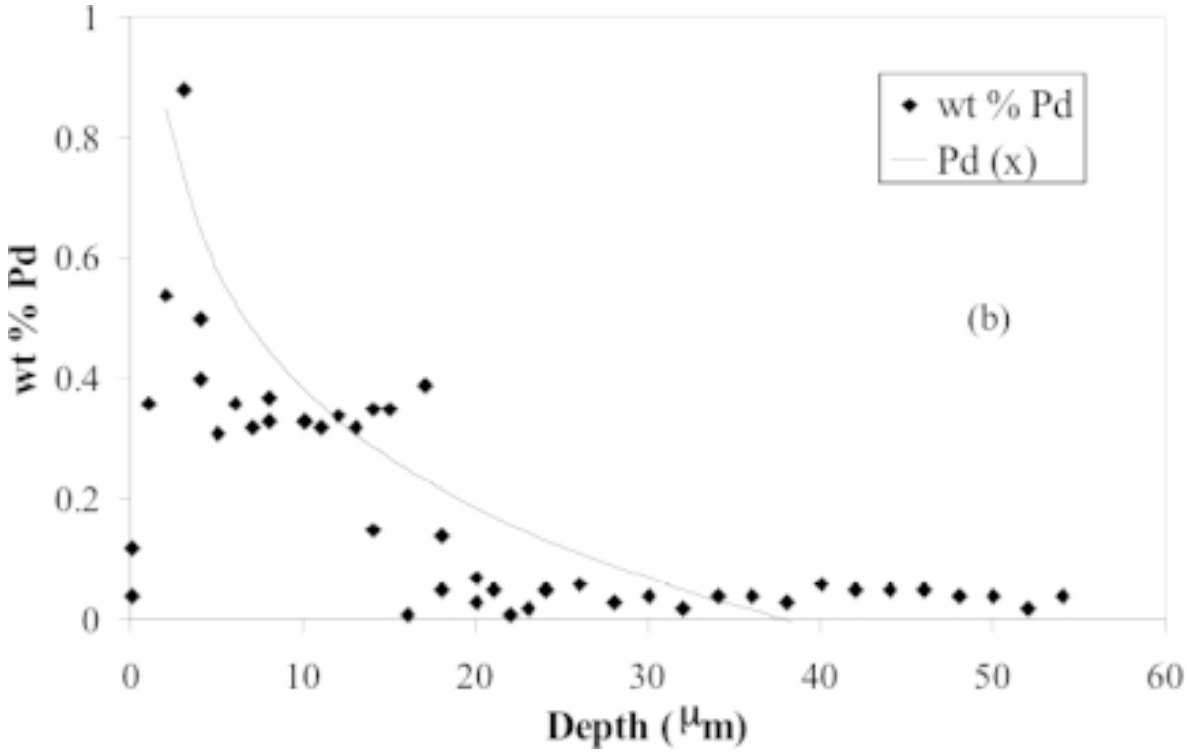

Fig. 3. Pd deposition profile obtained by EPMA and the mathematical model curve with l = 0.6 in the 5-Ti-5 nm membrane ([Pd] = 0.86 g/L in palladium acetate impregnation solution).

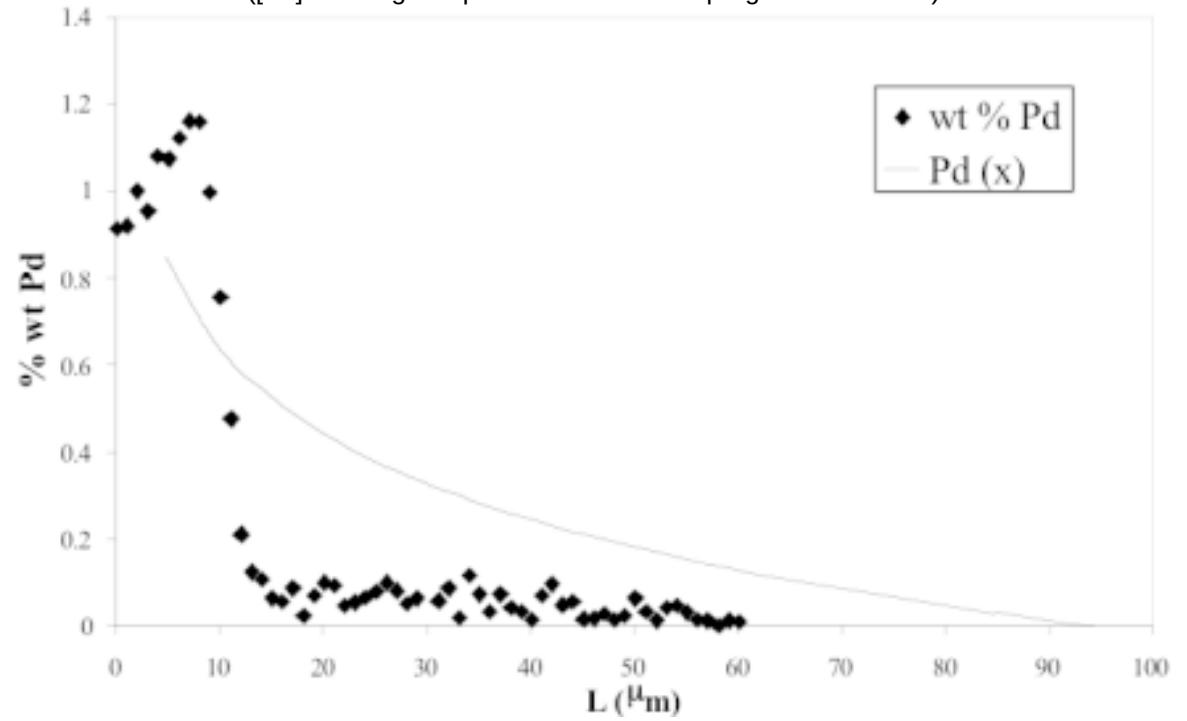

Fig. 4. Pd deposition profile obtained by EPMA and the mathematical model curve with l = 0.6 in the 6-Ti-5 nm membrane ([Pd]= 2.17 g/L in palladium acetate impregnation solution).

Pd-TiO_2-100 nm, respectively. For these two membranes, the calculated deposition profiles overestimate the Pd concentration in the first 10-20 microns depth.

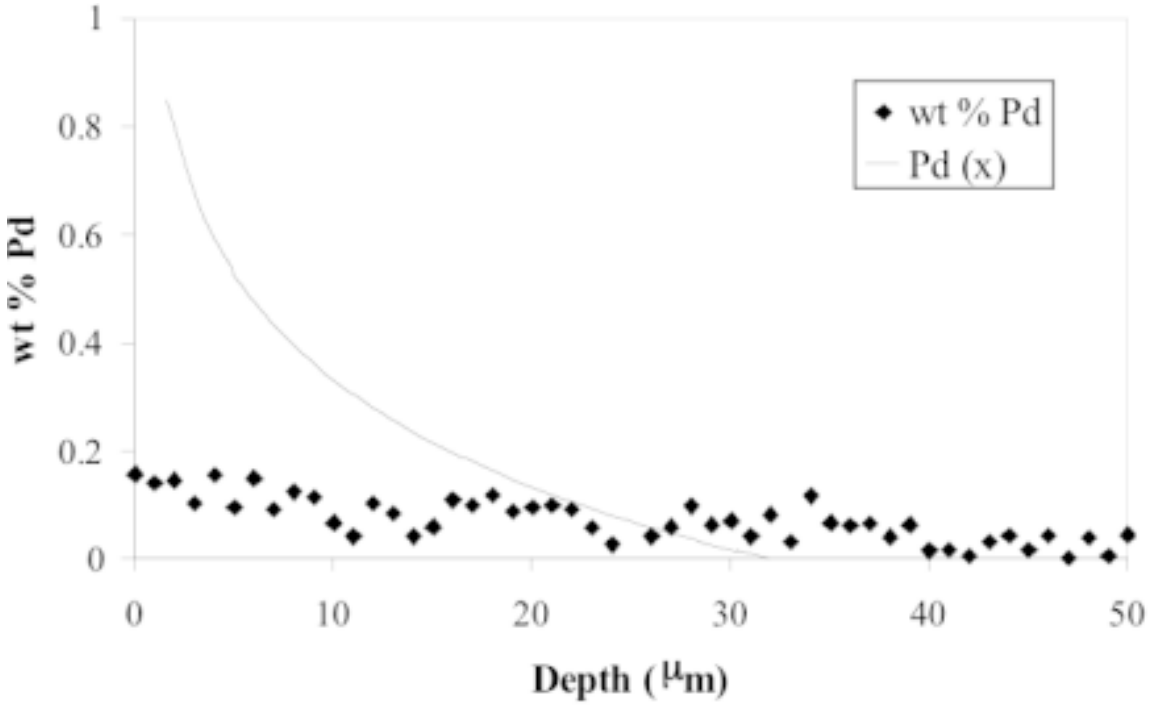

Fig. 5. Pd deposition profile obtained by EPMA and the mathematical model curve with l = 0.5 in the 7-Ti-30 nm membrane.

4.3.1.2. Bimetallic membranes (Pd-Cu, Pd-Zn)

The quantification of metals deposited in the alumina supports by EDS was less accurate than that obtained on titania-based supports, because the samples for microscopy were not polished, and the porosity of the support interferes with X-ray analysis. Therefore, the model presented in Section 3 was not applied in the case of samples 1-Al-5 nm, 2-Al-10 nm and 4-Al-25 nm.

Pd-Cu/Al_2O_3 – 5 nm membrane (sample 1-Al-5 nm, Pd/Cu= 1.15 in solution)

EDS analyses performed in different positions of the inner side of the tube (γ-Al_2O_3 layer) give an average Pd/Cu atomic ratio of 0.85, which is slightly lower than the ratio in the starting precursors solution (1.15). However, this value is in very good agreement with the chemical analyses of the inside layer given in Table 6 (8 mg Pd and 6 mg Cu correspond to an atomic ratio Pd/Cu= 0.8).

EDS line-scan analysis of Pd and Cu deposition profiles in the 1-Al-5 nm membrane cross-section is shown in Fig. 7a. As observed with the 5-Ti-5 nm and 6-Ti-5 nm membranes (Fig. 3 and Fig. 4), metals enrichment towards the γ-Al_2O_3 top layer is clearly evidenced.

The Pd/Cu ratio (Fig. 7b) is very low at depths >50 μm, but these values are not highly reliable since the amounts of metals analysed in this zone are very low (<0.1 wt.% for Pd). Between 0 and 30 μm, the metals concentration increases and the Pd/Cu atomic ratio found close to 1 are consistent with that of the precursors solution (1.15).

Pd-Cu/Al_2O_3 – 10 nm membrane (sample 2-Al-10 nm, Pd/Cu= 2.6 in solution)

The metals deposition profile in the 2-Al-10 nm membrane (Fig. 8) is more flat than in the case of the Pd-Cu/Al_2O_3 – 5 nm membrane (Fig. 7).

Metal enrichment becomes significant only in the first 10 μm close to the mesoporous top layer. The Pd/Cu ratio is ≈ 2.5 in the top layer, which agrees well with the Pd/Cu ratio in the precursor solution.

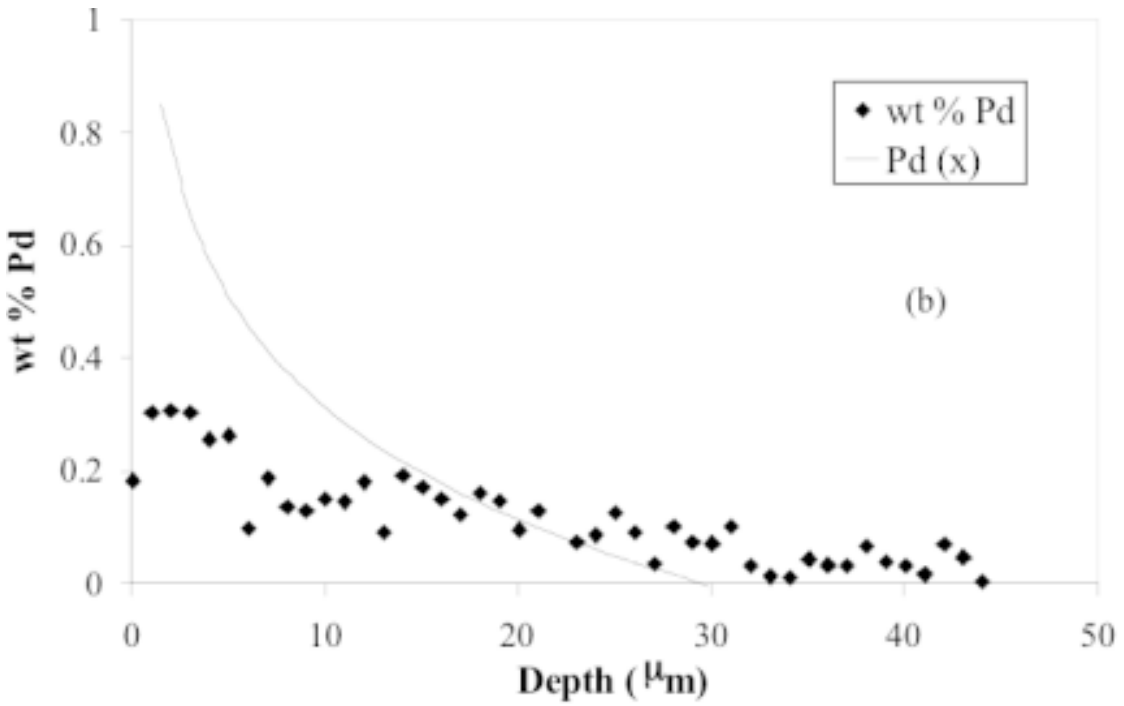

Fig. 6. Pd deposition profile obtained by EPMA and the mathematical model curve with l = 0.35 in the 8-Ti-100 nm membrane.

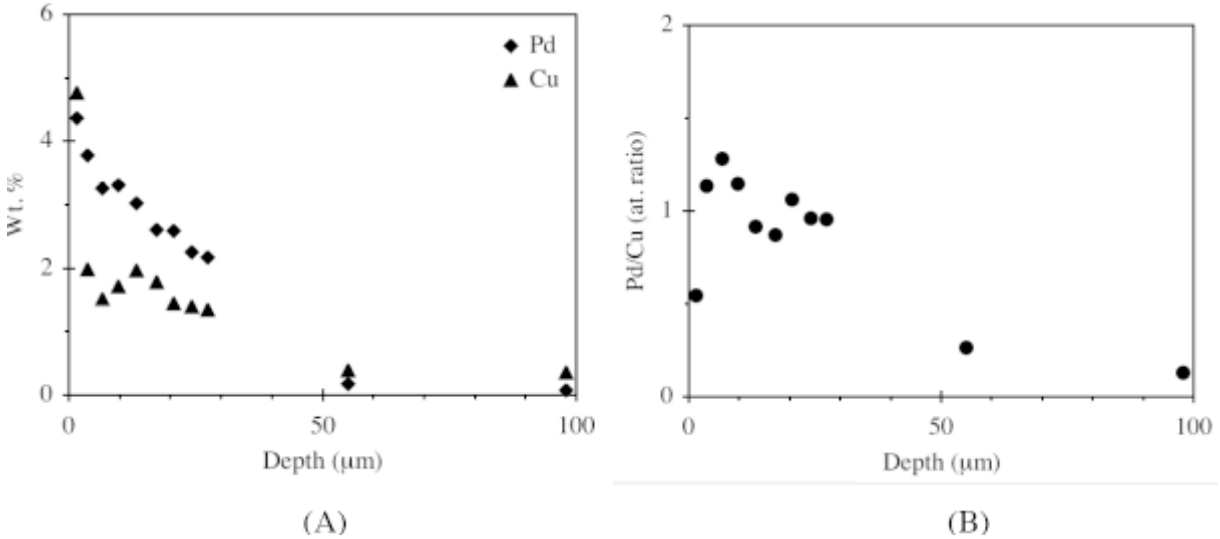

Fig. 7. Line-scan analysis of the 1-Al-5nm membrane cross-section. (A) Pd and Cu deposition profiles; (B) Pd/Cu atomic ratios calculated from EDS analyses. The depth is the distance between the inner side of the tube (γ-Al_2O_3 top-layer) and the position of the EDS probe.

Pd-Cu/Al_2O_3 – 25 nm membrane (sample 4-Al-25 nm, Pd/Cu= 2.6 in solution)

Again, the metals deposition profile in the 4Al-25 nm membrane (Fig. 9) appears more flat than in the case of the 1-Al-5 nm membrane (Fig. 7). Pd enrichment becomes significant only in the first 20 mm, and Cu enrichment only in the top layer.

The calculated Pd/Cu atomic ratio is in the range 2.5 - 2.7 in the γ-Al_2O_3 top-layer, in agreement with the Pd/Cu ratio in the precursors solution. The values calculated farther from the top layer are not highly reliable since the amount of Cu analyzed is

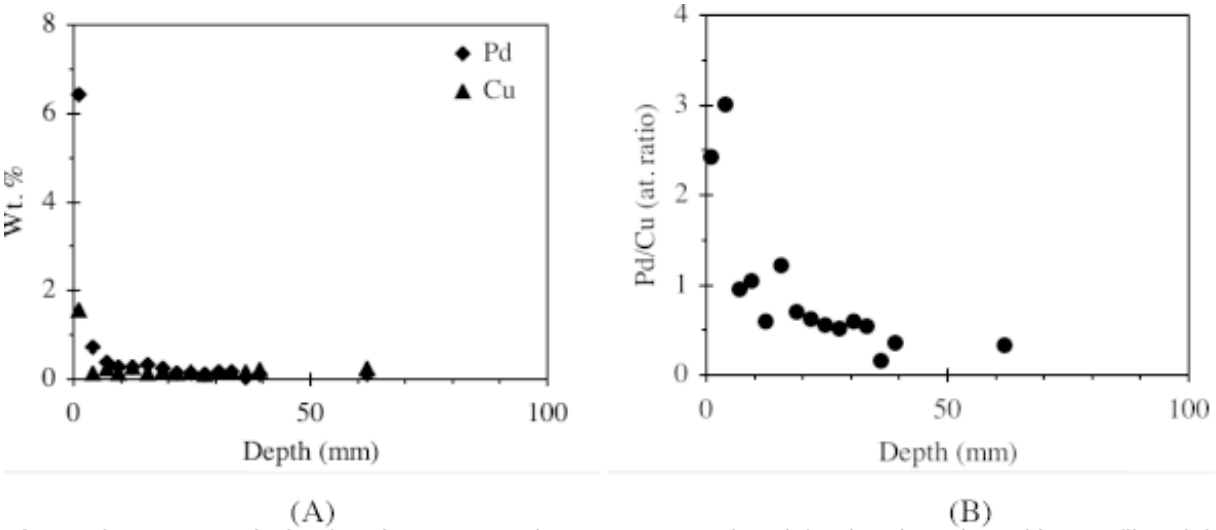

Fig. 8. Line-scan analysis of 2-Al-10 nm membrane cross-section. (A) Pd and Cu deposition profiles; (B) Pd/Cu atomic ratios calculated from EDS analyses. The depth is the distance between the inner side of the tube (γ-Al_2O_3 top-layer) and the position of the EDS probe.

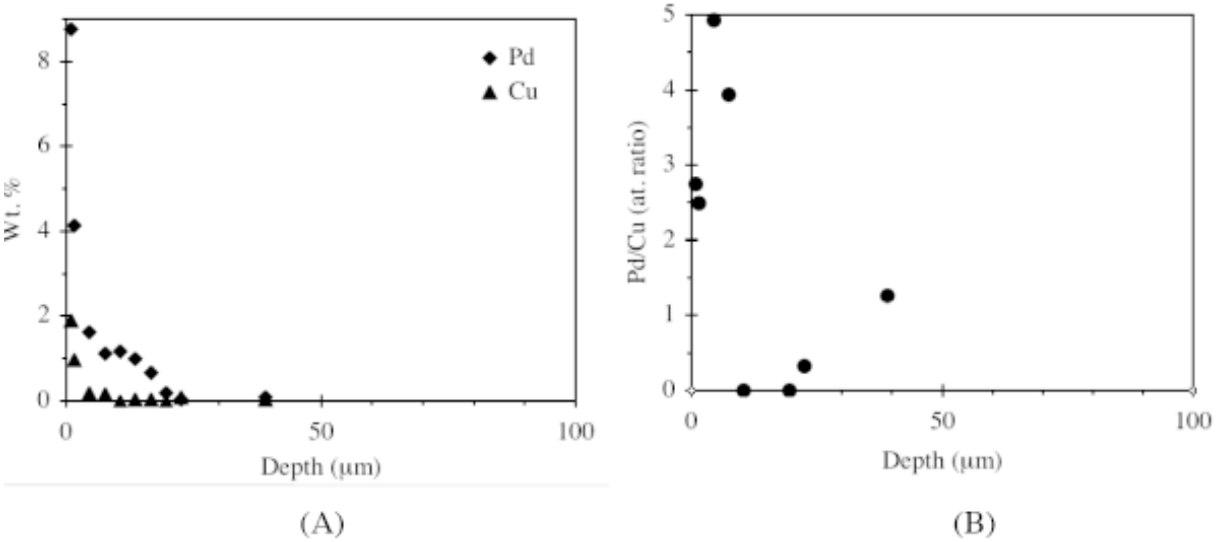

Fig. 9. Line-scan analysis of 4-Al-25 nm membrane cross-section. (A) Pd and Cu deposition profiles; (B) Pd/Cu atomic ratios calculated from EDS analyses. The depth is the distance between the inner side of the tube (γ-Al_2O_3 top-layer) and the position of the EDS probe.

very low (≈ 0.05 wt.%) and close of the detection limit of this technique.

Pd-Zn/TiO_2-5 nm membrane

The palladium and zinc deposition profiles are shown in Fig. 10. The palladium deposition profile is rather similar to that observed in the Pd/TiO_2-5 nm membrane (Fig. 3). In the present case, palladium is mainly located in the 20 μm depth, whereas zinc appeared more broadly distributed until 50 μm depth. This suggests that the zinc acetate solution reaches the saturation volume before the palladium acetate solution, in line with the higher concentration of the Zn precursor solution. The mean integral of the experimental curves considering 20 mm depth indicated Pd 0.1 wt.% and 1.2 wt.% Zn.

4.3.2. XPS analysis of the mesoporous surface of membranes

The Pd-Cu/Al_2O_3 membranes were analysed by XPS on the inner sides of the tubes. The depth

Table 8. XPS quantitative analysis of inner sides (γ-Al_2O_3 mesoporous layer) of the membranes, and calculated Pd/Cu atomic ratios from XPS analyses. For comparison, Pd/Cu atomic ratios determined by chemical analysis of impregnation solutions and by EDS analysis of inner sides of the tubes are included (analyses on ≈ 1-μm depth).

Sample	Pd/Al_2O_3 (wt.%)	Cu/Al_2O_3 (wt.%)	Pd/Cu (at. ratio, XPS, ≈ 5 nm)	Pd/Cu (at. ratio) in solution	Pd/Cu (at. ratio, EDS, ≈ 1 μm)
1-Al-5 nm	18.8	27.4	0.4	1.15	0.9
2-Al-10 nm	13.1	4.2	1.8	2.6	2.4
3-Al-10 nm	5.4	1.2	2.6	3.7	3.4
4-Al-25 nm	16.7	5.0	2.0	2.6	2.1

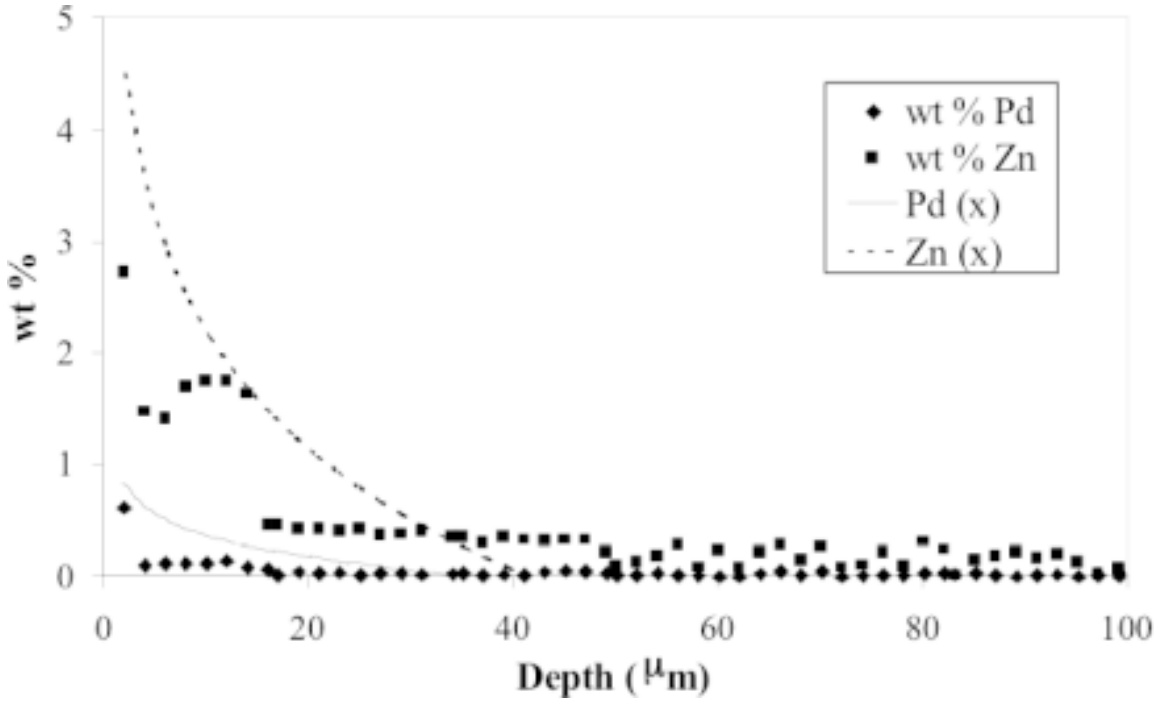

Fig. 10. Pd and Zn deposition profiles obtained by EPMA and deposition model curve with *l* = 0.4 for Pd and *l* = 0.5 for Zn in Pd-Zn/TiO2-5nm membrane.

analyzed is ≈ 5 nm, with analysis slots of 700x300 μm. Quantitative analysis of surface Pd and Cu (referred to alumina) and surface atomic ratios are reported in Table 8. For comparison, the Pd/Cu atomic ratios in the precursors solution are included.

XPS analyses reveal a very strong enrichment in metals at the surface of the tubes in both metals. For comparison, the global metal contents analysed by chemical analysis are in the range 0.067-0.17 wt.% for Pd, and 0.025-0.045 wt.% for Cu.

The surface Pd/Cu ratios measured by XPS (analysis on ≈ 5 nm depth) are systematically lower than those in the precursors solution, which suggests that the surface is more enriched in Cu than in Pd. They are also lower than the Pd/Cu ratios analysed by EDX in the first micron of the mesoporous top-layer (Table 8). This is probably related to the very high solubility of Cu nitrate in

water (1450 g/L [14]), which should lead to further concentration of copper nitrate towards the surface during the evaporation process while Pd nitrate has already reached the saturation concentration and precipitated.

5. DISCUSSION

5.1. Characterisation of metals distribution and specific requirements in the preparation of bimetallic catalytic membranes

A prerequisite in the preparation of catalytic membranes is that the porous system is not clogged by the deposited catalysts. As can be seen in Table 4, the nitrogen permeance is not significantly modified after metals deposition. With monometallic membranes, the amount of Pd deposited per tube is low (<4 mg), and therefore this result is not surprising. In the case of bimetallic membranes, the amount of metals per tube is significantly higher (35 to 48.6 mg, Table 5), which represents approximately the same mass as that of the mesoporous γ-Al_2O_3 top-layer (40 to 50 mg of alumina in a 25-cm long tube). However, Table 6 and Table 7 show that the largest amount of metals is actually deposited in the macroporous zones of the tube, and therefore the permeance is unaffected.

The cross-section metals distribution in the ceramic tubes was characterized by SEM-EDS profile analyses, chemical analysis and XPS. Although some analyses were performed close to the detection limit of the technique, the three techniques agree on a concentration of metals close to the mesoporous inner layer of the tubes. This trend was previously observed in the case of monometallic (Pt) catalytic membranes [16], and is confirmed in the present work with bimetallic membranes.

For instance in the case of alumina supports, although a large amount of Pd and Cu are deposited in the *intermediate* and *outside* zones, Tables 6 and 7 show that the metals concentration is always much higher in the *inside* zone, close to the mesoporous top layer. This is confirmed, to a variable extent, in all EDS profiles analyses. XPS analyses (Table 8) also reveal that Pd and Cu enrichment continues up to the top layer surface. A similar surface Cu enrichment was previously evidenced by SIMS experiments on powder Pd-Cu/Al_2O_3 catalysts [17]. This concentration should favourably affect the activity of the catalytic membranes, since there is a closer contact between the catalyst and the reactants in small pores.

As regards the preparation of bimetallic catalytic membranes, the relative ratio of the two metals is also a very important parameter, since it significantly influences the catalytic activity. As an example, the activity of supported Pd-Cu/Al_2O_3 catalysts in nitrates hydrogenation was found maximum at an atomic ratio Pd:Cu $\approx$ 1 [17], although other authors found this optimum at Pd:Cu $\approx$ 2 [18]. The different cross-section characterisations of tubes reveal that the Pd/Cu ratio varies significantly according to the position analysed. The atomic ratio of the impregnation solution is actually respected only in zone close to the γ-Al_2O_3 top layer (Fig 6-8). Since the catalytic reactions will essentially take place in the mesoporous top-layer, the respect of the targeted metal ratio is critical in this zone.

5.2. Effect of pore size on capillary flows during deposition-precipitation of metal precursors

During the deposition-precipitation method used in the preparation of catalytic membranes, the tubes were impregnated by a solution of metals precursors, followed by drying. According to [19], the drying step of a porous system can be characterized by a dimensionless parameter, α, which represents the ratio between the rate of capillary movements of the liquid in the pores (J_0^{cap}) and the rate of vapour removal (J_0^{vap}) (Eq. (3):

$$\alpha = \frac{J_{cap}^0}{J_{vap}^0} = \frac{\varepsilon.\sigma_{liq}.\rho_{liq}.\bar{r}.\Delta.\cos\theta}{4\beta.\mu_{liq}.D_1.\rho_{vap}.(\mathrm{Nu})} \qquad (3)$$

with:

ε = specific porosity of the support,

β = coefficient of pore tortuosity,

$\bar{r}$ = mean pore radius,

Δ = dispersion of the pore distribution, for uniform distribution $\Delta = (r_{max}-r_{min})/r_{moy}$,

θ = wetting angle,

σ_{liq} = surface tension of the liquid,

μ_{liq} = viscosity of the solution,

ρ_{liq}, ρ_{vap} = density of the solution, density of the vapour,

D_1 = coefficient of vapour molecular diffusion,

Nu = Nusselt number,

When α<<1, the drying regime is fast, which means that evaporation is rapid compared to the capillary flow, leading to the penetration of an evaporation front inside the porosity of the support.

Table 9. Dimensionless parameter, α, characterising the drying regime in alumina and titania tubes, during the evaporation of precursors solutions.

Support	Impregnation solvent	α
Al_2O_3 – 5 nm	Water	0.06
Al_2O_3 – 10 nm	Water	0.12
Al_2O_3– 25 nm	Water	0.30
TiO_2 – 5 nm	Acetone	0.02
TiO_2 – 30 nm	Acetone	0.12
TiO_2 – 100 nm	Acetone	0.41

The concentration of the solution increases with solvent evaporation, and a precipitate forms when the saturation concentration has been reached, or when the total solvent volume decreases down to the saturation volume V_s, as described in the model of section 3. In contrast, when a>>1 (slow drying), the vapour removal is slow compared to capillary flows. The evaporation boundary shifts through wide pores. When the liquid domains become disconnected, the solution remains in isolated domains, which will result in metal precursor precipitation everywhere in the porosity, before the solvent volume decreases down to V_s.

In order to characterize the drying regime in the catalytic membranes prepared, we calculated this α parameter for the different tubes (Table 9), considering in the calculation only the influence of the inner layer (mesopores of 5, 10, and 25 nm for Al_2O_3 membranes prepared with water as the solvent, and pores of 5, 30, and 100 nm for TiO_2 membranes prepared with acetone as the solvent). The capillary movements and evaporation in the macroporous layers were considered as similar in the two types of tubes.

In all cases we find α<1 (Table 9), with α<<1 (rapid drying) for the smallest pores. α tends to increase with pore size and is higher, at comparable pore size, with alumina tubes (prepared in water solution) than in titania tubes (prepared in acetone). This suggests that the capillary transfer is always slower than the solvent evaporation, and that this difference in flow rates increases when the pore size decreases: since capillary forces are higher in small pores, the liquid is more strongly trapped and therefore less mobile. According to Eq. (3), an increase of α should be related to an increase of the capillary flow and/or a decrease of the vapour flow. Since a decrease of vapor removal rate when the pore size increases is unlikely (on the contrary, evaporation should be easier when the pore size increases), the most pronounced effect of the pore size is probably related to the capillary flows: when the pore size increases, the liquid moves more easily, which results in higher capillary flows.

This parameter agrees well with the deposition profiles analyzed by SEM-EDS (Figs. 4 to 9). As long as the same impregnation solvent is concerned, i. e. acetone and TiO_2 membranes, the impregnation profile is more homogeneous in the tubes with 30 and 100 nm pores (see Fig. 3 to 5) because the drying regime is slower, and allows the metal precursors to precipitate within the hole thickness of the tube. In the 5 nm pores tube (Fig. 3), the palladium concentrates mainly in the first 20 mm because the liquid is strongly sucked towards the mesoporous layer, and evaporation takes place within the tube thickness with practically no Pd deposition until saturation is reached.

For alumina tubes, catalytic membranes with top-layer pores of 5, 10, and 25 nm were prepared and characterized. Due to the combination of solvent and support properties, the drying regime is always “slower”, at similar pore size, than that of titania tubes. Under these conditions, a concentration of metals towards the γ-Al_2O_3 mesoporous layer is evidenced whatever the pore size. Moreover, the Pd and Cu nitrate precursors used to prepare the alumina tubes are much more soluble in water than Pd acetate in acetone (solution used for the preparation of TiO_2 membranes), which could allow the nitrates solution to concentrate strongly in the mesoporous layer during the evaporation process.

5.3. Model of precursors deposition in the membranes by evaporation crystallization

The deposition model described in Section 3 was applied to predict the influence of metal concentration in the precursor solution on the catalyst distribution in the membrane crosssection. As an example, Fig. 11 shows different theoretical deposition curves of Pd acetate deposition at different concentrations. The model predicts that doubling the metal concentration (7 to 14 g/L) in solution should lead to a limited increase of the Pd weight uptake in the first microns (0-5 mm) of the membrane depth. It also shows that, in order to double the weight uptake in this zone, the Pd concentra-

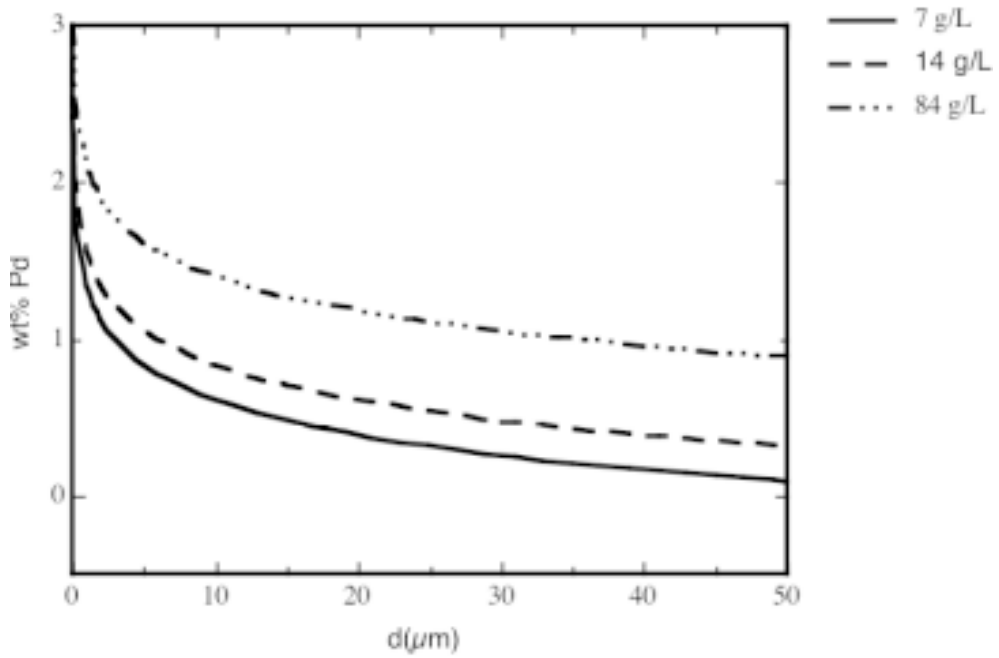

Fig. 11. Deposition profile of Pd as a function of Pd concentration in the precursor solution calculated by the model.

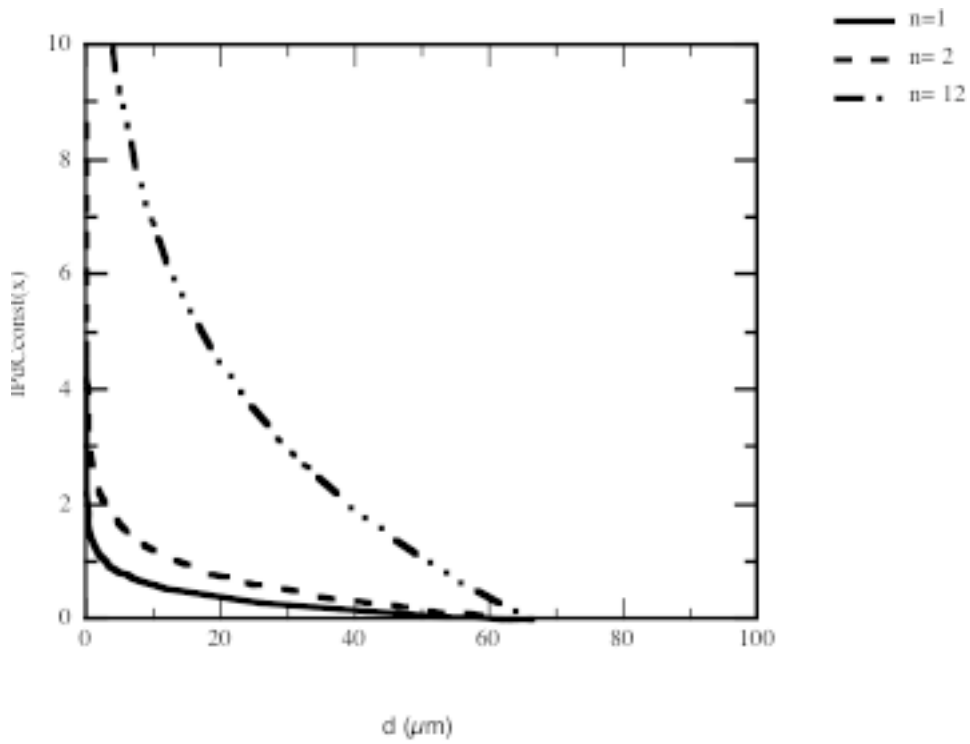

Fig. 12. Predicted Pd deposition after 1, 2 and 12 successive impregnation steps with [Pd]=7g/L in the precursor solution.

tion in solution should be increased by a factor of 12.

According to the model, another option to obtain a membrane with an increased metal amount close to the top-layer is to perform successive impregnations steps, separated by decomposition of the metal precursor in order to avoid any re-dissolution of the salt. This is shown in Fig. 12, where

the number of impregnation steps is varied from 1 to 12. In this case, the impregnation steps are cumulative and the amount of metal in the top-layer is proportional to the number of impregnations.

5.4. Critical assessment of the deposition model of metals in the membranes

The simple mathematical model chosen to describe the metals deposition in the membranes includes two assumptions:

(i) the solvent does not evaporate from the internal top-layer,

(ii) the solvent and solutes migrate towards the smallest pores, i.e. the inner layer of the tube.

This model predicts that the precursor solution will concentrate towards the smallest pores during the evaporation process, leading to metals deposition in this zone. However, the model does not include any hypothesis on the effect of pore size on the drying process, which eventually has a strong impact on the relative rates of capillary and vapour flows, as can be seen from the calculation of α (Table 9).

The deposition profile predicted by the model in the previous section can match the experimental data, for some membranes (Fig. 3, Fig. 4, Fig. 10). In these cases (TiO_2 5 nm and Al_2O_3 membranes), the hypotheses behind the model appear verified. However, in some other cases, the matching is difficult (Fig. 6) or even very poor (Fig. 5). The top-layer pore size is actually the largest in these two tubes, which suggests a relationship between this pore size and the deposition profile. The two hypotheses of the model imply that an evaporation front penetrates the membrane thickness and that the precursors solution concentrates towards the smallest pores (α small). The model actually matches well the deposition profiles in these cases. However, when α increases, the hypotheses behind this model are not verified anymore. This suggests that the capillary forces and other physical phenomena, in particular the diffusivity of the metal salts [20], should be taken into account for a more general to description of the observed deposition profiles.

6. CONCLUSIONS

Wet impregnation of porous multilayer ceramic tubes by the evaporation-crystallization method was investigated to prepare mono- and bi-metallic catalytic membranes. The metal deposition was characterized by several techniques. A tentative mathematical model describing the precipitation of metal precursors during drying was tested. The following conclusions can be drawn from the obtained results:

- A strong metal concentration in the lumen side of the tubes, close to the top-layer, was evidenced in all tubes with the smallest top-layer pore size (5-25 nm). On the contrary, this concentration is very moderate when the top-layer pore size increases.
- Metals concentration is observed in the case of bimetallic membranes, prepared either by simultaneous or successive impregnation.
- The top-layer pore size strongly influences the deposition profile, apparently by modifying the rate of capillary flows during the drying step.
- The model matches fairly well the analysed deposition profiles in membranes exhibiting the smallest top-layer pore size (5-25 nm). However, when larger pores were concerned, other parameters, including capillary flows and diffusivity of metal precursors, should be taken into account. A complete model describing the specific features of the drying of porous membranes, (two ends pores), should be developed.

ACKNOWLEDGEMENTS

The authors thank the Région Rhône-Alpes (Cluster 5 - Procédés et environnement) and the French-Lebanon Program CEDRE for funding this work. The contributions of F. Beauchesne-Simonet to ESEM measurements and of L. Massin to XPS analyses, and the fruitful discussions with Marc Pera-Titus are gratefully acknowledged.

ANNEX

Calculation of α:

Specific porosity of the support: $\varepsilon = 0.25$

Coefficient of pore tortuosity $\beta = 1.3$

Mean pore radius $\bar{r} = 2.5 \cdot 10^{-9}$ or $5 \cdot 10^{-9}$ or $1.25 \cdot 10^{-8}$ or $1.5 \cdot 10^{-8}$ or $5 \cdot 10^{-8}$ m

Dispersion of the pore distribution $\Delta = 1$

Wetting angle $\theta = 0°$

Surface tension of the liquid $\sigma_{liq} = 0.072$ Nm^{-1} for water and 0.0235 Nm^{-1} for acetone

Viscosity of the solution $\mu_{liq} = 8.9 \cdot 10^{-4}$ Pa·s for water and $3.06 \cdot 10^{-4}$ Pa·s for acetone

Density of the solution $\rho_{liq} = 997.05$ kg·m^{-3} for water and 784.5 kg·m^{-3} for acetone

Density of the vapour $\rho_{vap} = 0.804$ kg·m^{-3} for water and 2.41 kg·m^{-3} for acetone

Coefficient of vapour molecular diffusion D_1 = $2.42 \cdot 10^{-5}$ $m^2 s^{-1}$ for water and $1.04 \cdot 10^{-5}$ $m^2 s^{-1}$ for acetone

Nusselt number $Nu = 2 + 1.8 Re^{1/2} Pr^{1/3}$

Reynolds number $Re = \rho_{vap}.v.l/\mu_{vap}$

With:

Vapour rate $v = 3.14 \cdot 10^{-2}$ $m \cdot s^{-1}$ (rotation rate of the tube during drying)

Characteristic length $l = 5 \cdot 10^{-3}$ m (radius of the tube)

Viscosity of the vapour $\mu_{vap} = 10^{-5}$ Pa·s for water and $7.6 \cdot 10^{-4}$ Pa·s for acetone

Prandtl number $Pr = \mu_{vap}.C_p/\lambda_{vap}$

With:

Specific heat capacity of vapour C_p = 1850 $J \cdot kg^{-1} K^{-1}$ for water and 1293 $J \cdot kg^{-1} \cdot K^{-1}$ for acetone

Thermal conductivity of vapour λ_{vap} = 0.0187 $W \cdot m^{-1} \cdot K^{-1}$ for water and 0.0115 $W \cdot m^{-1} \cdot K^{-1}$ for acetone

Which gives:

Re = 12.63 for water and 49.81 for acetone

Pr = 0.989 for water and 0.855 for acetone

Nu = 8.37 for water and 14.05 for acetone

REFERENCES

[1] F. Gauthard, F. Epron and J. Barbier // *J. Catal.* **220** (2003) 182.

[2] J. Sá and H. Vinek // *Appl. Catal. B-Environ.* **57** (2005) 247.

[3] M. Reif and R. Dittmeyer // *Catal. Today* **82** (2003) 3.

[4] A. Bonilla Sànchez, N. Homs, J.L.G. Fierro and P. Ramírez de la Piscina // *Catal. Today* **107-108** (2005) 431.

[5] J.A. Dalmon, In: *Handbook of Heterogeneous Catalysis*, ed. by G. Ertl, H. Knözinger and J.Weitkamp (VCH Publ., 1997), Chapter 9.3, p. 1387.

[6] A.V. Neimark, L.I. Kheifez and V.B. Fenelonov // *Ind. Eng. Chem. Prod. Res. Dev.* **20** (1981) 439.

[7] D. Uzio, S. Miachon and J.-A. Dalmon // *Catal. Today* **82** (2003) 67.

[8] K. Daub, G. Emig, M.-J. Chollier, M. Callant and R. Dittmeyer // *Chem. Eng. Sci.* **54** (1999) 1577.

[9] O.M Ilinitch, F.P. Cuperus, L.V. Nosova and E.N. Gribov // *Catal. Today* **56** (2000) 137.

[10] R. van der Vaart, V.I. Lebedeva, I.V. Petrova, L.M. Plyasova, N.A. Rudina, D.I. Kochubey, G.F. Tereshchenko, V.V. Volkov and J. van Erkel // *J. Membrane Sci*. **299** (2007) 38.

[11] D.M. Dotzauer, J. Dai, L. Sun and M.L. Bruening // *Nano Lett.* **6** (2006) 2268.

[12] M. Vospernik, A. Pintar, G. Bercic, J. Levec, J. Walmsley, H. Ræder, E.E. Iojoiu, S. Miachon and J.-A. Dalmon // *Chem. Eng. Sci.* **59** (2004) 5363.

[13] A.K. Yatsimirsky, A.D. Ryabov, V.P. Zagorodnikov, I.K. Sakodinskaya, O.I. Kavetskaya and I.V. Berezin // *Inorg. Chim. Acta* **48** (1981) 163.

[14] David R. Lide, *CRC Handbook of Chemistry and Physics, 84th Edition* (CRC, 2003-2004).

[15] S. Yan, H. Maeda, K. Kusakabe and S. Morooka // *Ind. Eng. Chem. Res.* **33** (1994) 616.

[16] E.E. Iojoiu, J. Walmsley, H. Ræder, R. Bredesen, S. Miachon and J.A. Dalmon // *Rev. Adv. Mater. Sci*. **5** (2003) 160.

[17] O.M. Ilinitch, L.V. Nosova, V.V. Gorodetskii, V.P. Ivanov, S.N. Trukhan, E.N. Gribov, S.V. Bogdanov and F.P. Cuperus // *J. Mol. Catal. A-Chem*. **158** (2000) 237.

[18] J. Sá and H. Vinek // *Appl. Catal. B-Environ*. **57** (2005) 247.

[19] A.V. Neimark, L.I. Kheifez and V.B. Fenolov // *Ind. Eng. Chem. Prod. Res. Dev.* **20** (1981) 436.

[20] C. Galarraga, E. Peluso and H. de Lasa // *Chem. Eng. J*. **82** (2001) 13.